Available online at www.sciencedirect.com
SCIENCE DIRECT®
C. R. Physique 6 (2005) 997–1012
COMPTES RENDUS PHYSIQUE
http://france.elsevier.com/direct/COMREN/

Spintronics/Spintronique

Magnetic recording read head sensor technology

Jeffrey R. Childress *, Robert E. Fontana Jr.

Hitachi Global Storage Technologies, San Jose Research Center, 650 Harry Road, San Jose, CA 95120, USA

Abstract

Since the invention of the hard-disk drive in 1956, the technology of the magnetic head sensor has never ceased to evolve. Today's sensors are drastically different from those used in these early heads; they can detect and transmit information from recorded data at densities greater than 200 Gbit/in^2 and data rates approaching 1 GHz. Numerous advances in nanomagnetics, magnetic ultrathin films, magneto-electronics, as well as device processing, have fueled the remarkable progress of this technology. An overview of the science and technology behind magnetic read head sensors is presented. The dimensional, geometrical and magnetic requirements for the heads are first described, followed by a description of the state of the art giant-magnetoresistive read sensors. We then discuss characteristics and potential advantages of next-generation read sensors, including current-perpendicular-to-plane tunnel-magnetoresistance and giant magnetoresistive sensors. The interplay between sensor properties, size requirements, process limitations and head performance is emphasized. ***To cite this article: J.R. Childress, R.E. Fontana Jr., C. R. Physique 6 (2005).***

Résumé

La technologie des capteurs pour têtes de lecture magnétiques. Depuis l'invention du disque dur en 1956, la technologie des capteurs pour têtes de lecture magnétiques n'a cessé d'évoluer. Les capteurs actuels diffèrent profondément de ceux qui étaient utilisés dans ces premières têtes ; ils peuvent détecter et transmettre l'information de données enregistrées avec des densités supérieures à 200 Gbits/pouce carré, et ceci à des taux approchant 1 GHz. Ces progrès technologiques remarquables ont été alimentés par de nombreuses avancées en nanomagnétisme, en magnéto-électronique et en process des dispositifs. Nous présentons un panorama de la science et de la technologie des capteurs pour têtes de lecture. Nous décrivons tout d'abord les conditions que doivent remplir les têtes en termes de dimensions, de géométrie et de magnétisme, puis l'état de l'art en matière de capteurs de lecture à magnétorésistance géante. Nous discutons ensuite les caractéristiques et les avantages potentiels de la prochaine génération de capteurs de lecture, en particulier les capteurs à magnétorésistance tunnel et à magnétorésistance géante fonctionnant avec courant normal au plan. Nous soulignons l'interdépendance entre propriétés des capteurs, contraintes dimensionnelles, limitations des process et performances des têtes. ***Pour citer cet article : J.R. Childress, R.E. Fontana Jr., C. R. Physique 6 (2005).***

Keywords: Magnetic head sensor; Magnetoresistive read sensor

Mots-clés : Capteurs pour têtes de lecture magnétiques ; Capteurs de lecture à magnétorésistance

* Corresponding author.
E-mail address: jeff.childress@hitachigst.com (J.R. Childress).

1631-0705/$ – see front matter
doi:10.1016/j.crhy.2005.11.001

1. Introduction

It can be argued that the read sensor in the recording head of hard-disk drives (HDD), based on the phenomenon of giant magnetoresistance (GMR), was the first high-volume commercial example of true magnetic nanotechnology and spintronics. It also introduced a new level of complexity to the practical manufacture of microelectronic devices. The modern head sensor is indeed a complex device: The basic magnetoresistive film can be composed of a dozen or more layers of magnetic and non-magnetic materials whose effective thickness is controlled at the sub-Angstrom level. Each of these layers directly determine or affect the magnetic and magnetotransport behavior [1]. From this multilayer, a working sensor and head are created after over 250 processing steps, using techniques that are near the limits of current lithography, combining insulating and conducting materials, hard magnet biasing, and magnetic shielding. The final product needs to be compatible with the unforgiving fabrication and environment of recording heads designed to fly just a few nanometers above a spinning disk at up to 15 000 revolution per minute [2]. In this paper, we present an overview of magnetic read head (MRH) technology as it stands now, and how it might be expected to evolve in the future.

The key to understanding MRH technology is to grasp the geometrical and environmental constraints under which it operates. The recording head can be thought of having three main components: (1) the read sensor, which is the subject of this paper; (2) the write transducer (‘writer’), which is a microfabricated planar electromagnet with a narrow pole that creates a high density of magnetic flux in proximity to the media; and (3) the slider, which is a shaped piece of substrate (typically alumina-titanium carbide) onto which the writer and read sensor are built, and is engineered to ‘fly’ only a few nanometers above the spinning media disk. Here we only discuss the read sensor in detail. Therefore it is understood that for each example of sensor discussed below there is an appropriate combination of writer and slider which forms a coherent recording head device and, together with the chosen media, mechanical characteristics, and electronics, forms a complete recording system. Thus the recording environment in which the head is expected to operate is first introduced, including media characteristics, magnetic interference and shielding, and signal-to-noise (SNR) considerations. These constraints put specific boundaries on the sizes, geometries, and magnetic properties which a read sensor must achieve. This leads to a discussion of the nanotechnology inherent in recording heads, including thin-film MR technology, lithography and processing requirements, and magnetic domain control (sensor biasing) on the nanoscale. Then the status of current head technology (CIP-GMR) is discussed, together with potential alternatives (CPP-TMR and CPP-GMR). Finally possible future sensor technologies are explored.

2. Read heads in magnetic recording

2.1. The recording process

The magnetic recording process utilizes a thin film transducer for the creation or writing of magnetized regions (bits) onto a thin film disk and for the detection or reading of the presence of transitions between the written bits. The thin film transducer is referred to as a thin film head. It consists of a read element, the subject of this paper, which detects the magnetic bits and a write element which creates or erases the bits. Fig. 1 is a schematic of the recording process showing the media with written longitudinal bits, the transducer with a yoke-like electromagnet structure for writing bits, and a shielded magnetoresistive film structure for detecting the ‘out of disk plane’ stray fields emanating from the transitions. Fig. 2 shows a perspective view of the thin film head as viewed from the surface of the disk.

In a disk recording system, successive bits are written onto the disk surface in concentric rings or tracks separated by a guard band. The head transducer is attached to a suspension, and the suspension is attached to an actuator which controls the position

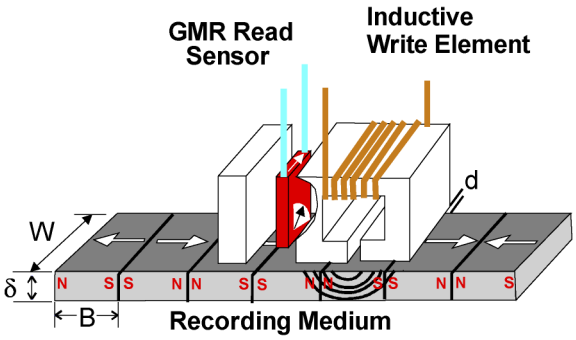

Fig. 1. Schematic of longitudinal recording process.

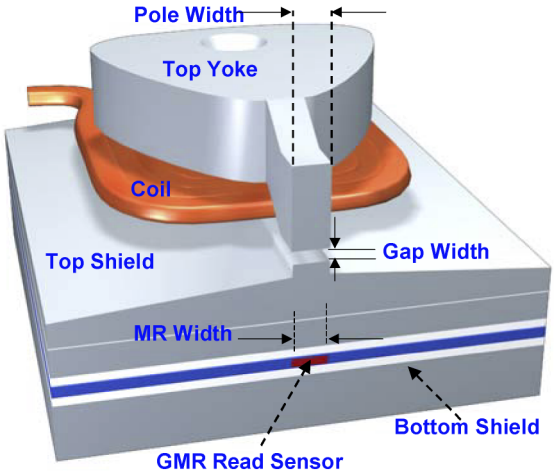

Fig. 2. Thin-film head structure as viewed from the media disk surface.

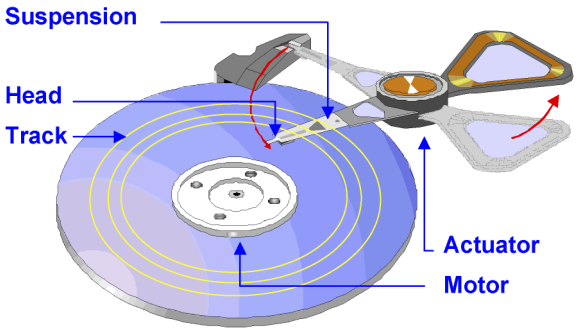

Fig. 3. Overall view of actuator and suspension (onto which the head is attached), and recorded tracks on the disk surface.

of the transducer in a plane above the disk surface. A specially-designed topography on the lower surface of the slider (known as the air-bearing surface or ABS) allows the head to 'fly' above the rotating disk (typically 4200–15 000 rpm), and controls the height of the transducer above the disk surface, typically 10 to 15 nm. Written tracks, the suspension, and the actuator are shown in Fig. 3.

2.2. Geometrical considerations

The bit geometry within a track are determined by the geometry of the thin film head. Areal density for a particular recording system is the product of the tracks per inch (TPI) in the cross-track direction and the bits per inch (BPI) within a track. Fig. 5 shows a write pole width (WW), a sensor width (RW), and a sensor gap separation between shields (TG). The width of the written bit is approximately equal to WW (but slightly larger due to fringing effects of the writing fields), and Fig. 4 shows the final bit geometry on the disk surface. The guard band width, or empty space between written tracks, is typically set at 20% of WW to isolate the bits from adjacent track transition interference. The sensor width RW is only about 60% of WW to allow for tolerance in the placement of the sensor over the written transition during the read or detection operation. Along the track direction, isolation of the sensor from fields emanating from transitions extraneous to the one being sensed is provided by two magnetic shields placed above and below the sensor with a total separation gap TG. Assuming that the read sensor has a linear response to the media field (see Section 3.2), then the presence of up to 2 transitions between the shields of the sensor can be simultaneously and accurately detected using advanced signal processing techniques [3]. Consequently the minimum allowable separation for magnetic transitions in a given track is 50% of TG. Table 1 shows critical dimensions and densities for a recording system supporting 80 Gbit/in^2 areal densities, nowadays a common density for notebook computer applications.

Table 1
Representative dimensions of the recording system for a hard disk-drive product with a real density of 80 Gb/in^2

Attribute–system	Value
Areal density	80 Gbit/in^2
Tracks per Inch (TPI)	100,000/in
Bits per Inch (BPI)	800,000/in
Attribute–transducer	
Write width	200 nm
Read width	120 nm
Guard band width	40 nm
Shield separation	60 nm
Track pitch	240 nm
Bit length	30 nm

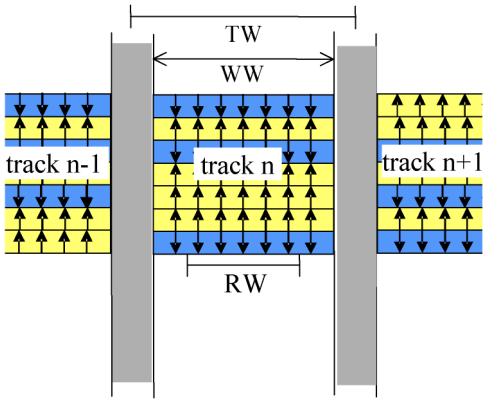

Fig. 4. Close-up view of recorded bits (blue (dark) and yellow (light)) with a recorded track. (For interpretation of the references to colour, the reader is referred to the web version of this article.)

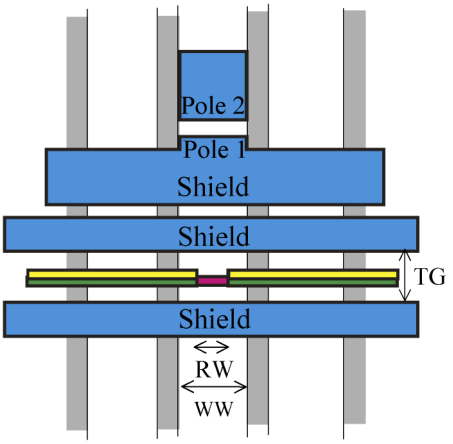

Fig. 5. Recording head dimensions compared to track dimensions on the disk.

3. Heads: from micro- to nano-technology

3.1. Recording densities and sensor dimensions

Nearly every read sensor in production today is of the giant magnetoresistive (GMR) type, in the so-called 'current-in-plane' (CIP) geometry (see Section 4). These sensors are composed of metallic thin-film multilayers of magnetic and non-magnetic materials, with the sensor current flowing in a direction generally parallel to the layers. Fig. 6 shows a scanning electron microscope image of the 'disk surface' view for a GMR-type thin-film head. The *minimum features* of the thin film head are the pole width (WW—green (upper) circle) and the sensor width (RW—red (lower) circle) (for colours see the web version of this article). Over the last 25 years advances in thin film processing have decreased the dimensions for these features with the result that areal densities in disk drive products have increased at annual rates of 50–60% per year, as shown in Fig. 8. Today, the minimum feature dimensions of the read width and write width of the thin film head have converged to the roadmap values for integrated circuit processing, 90 nm, with areal densities in excess of 120 Gbit/in^2 being achieved. Fig. 7(a) shows the values of RW and TG required for various area density targets, and Fig. 7(b) shows minimum feature history for both recording heads

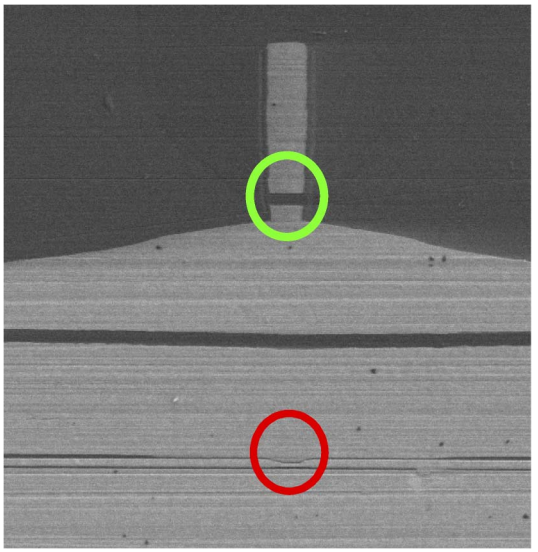

Fig. 6. SEM image of a recording head (as viewed from the disk), showing the write head gap (green (upper) circle) and the read element (red (lower) circle).

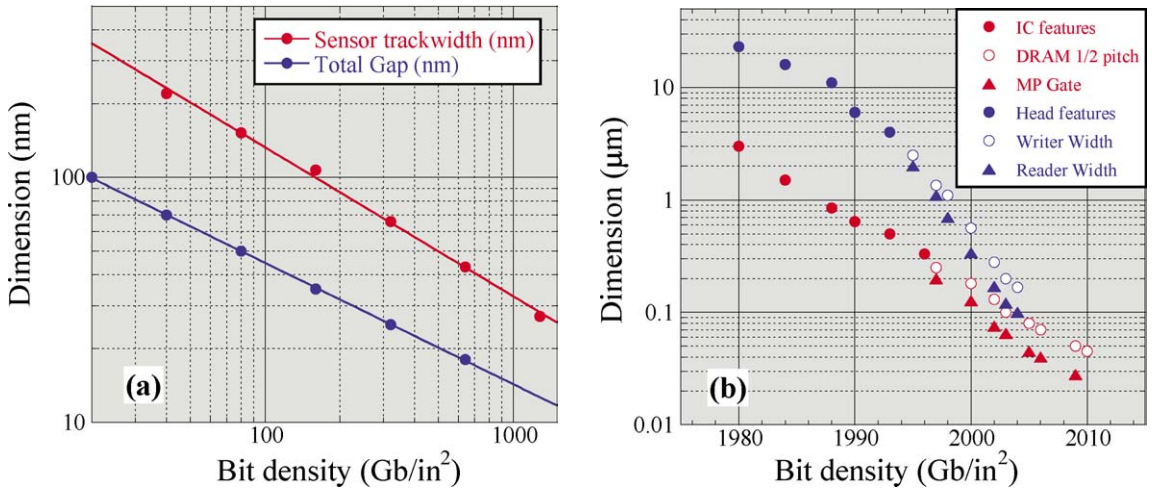

(a) (b)

Fig. 7. (a) Scaling estimate of head dimensions in terms of recorded bit density (Gbit/in^2), showing the sensor read width RW (red line) and shield-to-shield total gap spacing TG (blue line). (b) Actual evolution of head critical feature dimension over time (blue), compared to integrated chip (IC) technology critical dimensions (red).

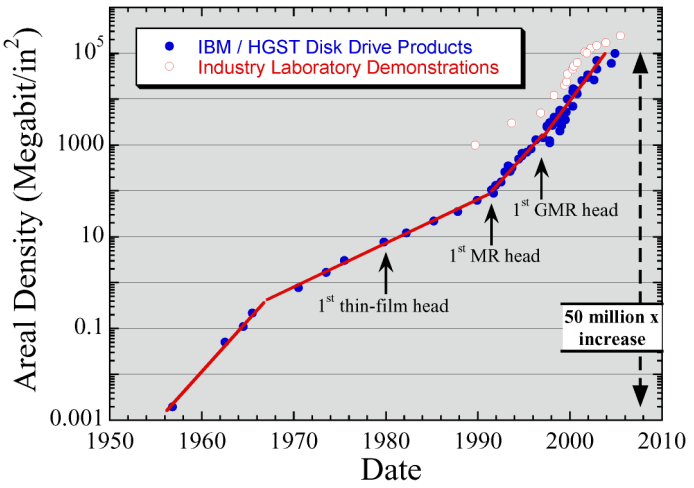

Fig. 8. A real-density growth curve of hard-disk drive recording products over time.

and semiconductor integrated circuits [4]. It can be seen that after consistently trailing the semiconductor roadmap by about 15 years, recording head processing now achieves similar performance levels. One significant advantage of head processing is the much smaller number of critical features per wafer, which make e-beam lithography a realistic path to further push the limits of processing technology for heads.

3.2. Sensor fabrication, stabilization, and shielding

Sustained areal density growth rate over time in recording products (Fig. 8) has depended critically on the ability to fabricate, with ever decreasing critical dimensions, the thin-film shielded sensor [5]. This sensor consists of four elements, shown in Fig. 9: shields, a magnetic field sensing region with a magnetoresistive thin-film multilayer (see Section 4), an electrical lead layer that conducts current to the films in the sensing region, and a stabilization layer that biases the sensing ferromagnetic layer in the sensor into a single domain state. The shields are thick (>200 nm), sputtered or electroplated soft magnetic material such as sendust (FeSiAl) or permalloy (NiFe). As mentioned above, the shield separation TG determines the minimum bit spacing and is well below 100 nm. The lead and hard bias layer are separated from the shield by gap insulators (typically Al_2O_3). Because

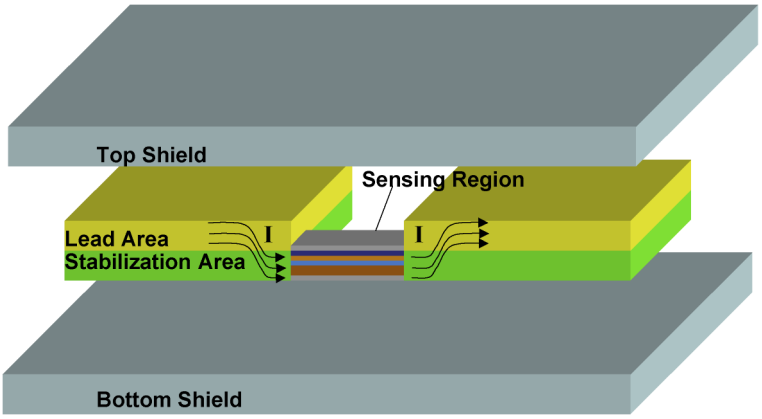

Fig. 9. Perspective view of lead region, hard magnet stabilization region, multilayer GMR sensing region, and top and bottom shields of a GMR head sensor.

the sensor is a two-terminal device, and because of the constricted path for the sense current between the shields, the lead material must have low resistivity (4–10 μΩ-cm) relative to the average resistivity of the sensor layers (25–50 μΩ-cm) in order to keep lead resistances to a reasonable value. Rh and Au are typical lead materials that meet this requirement, and result in a total lead resistance approximately equal to the sensor resistance. In order to accurately control the quiescent state of the free sensor layer and to eliminate hysteresis and Barkhausen noise due to domain structures, the sense ferromagnetic layer must be 'biased' by a small magnetic field (a few hundred oersteds). Bias stabilization of the ferromagnetic layer in the sense region is achieved when the fields from the *magnetized* hard ferromagnetic layer in the stabilization region, brought into close proximity to the ferromagnetic sense region layer, force the magnetization direction in this sense layer to align with the stabilization layer magnetization orientation [6,7]. The moment × thickness product, $M \times t$, of the stabilization layer is typically selected to be a factor of 4 to 8 times the $M \times t$ product of the ferromagnetic sense layer within the sensor stack. A CoPtCr film with a remnant magnetization $4\pi M_r$ of ∼ 5–10 kG is a typical hard ferromagnetic material used for sensor stabilization [8].

4. Giant-magnetoresistive (GMR) heads

4.1. Sensor magnetism and magnetoresistance

As explained in detail elsewhere in this issue, in magnetic multilayers the GMR signal comes from the change in electrical resistance that occurs when there is a change in the angle between two or more magnetic layers separated by a conducting

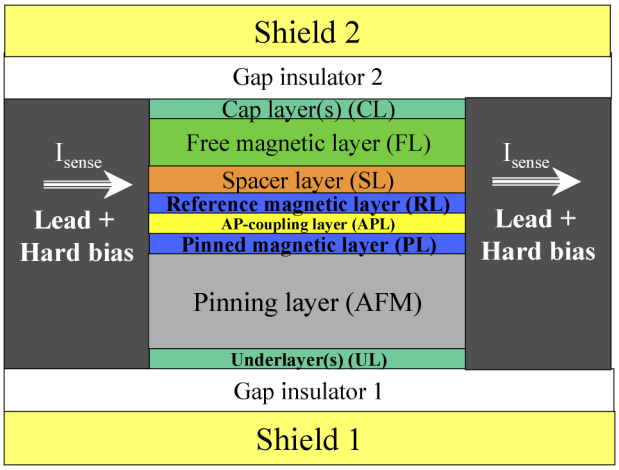

Fig. 10. Disk-view schematic of typical thin-film multilayer stack for CIP GMR sensor. The current flows horizontally between the lead/hard bias regions.

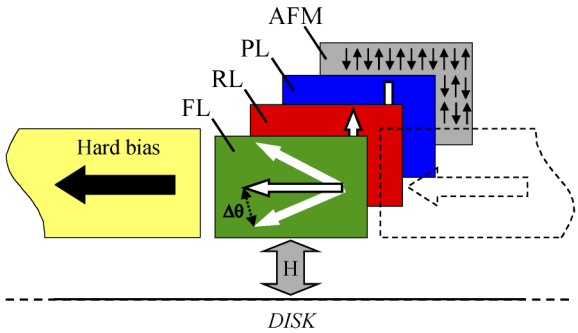

Fig. 11. Perspective view of the relative magnetization directions of the Hard bias, free sensing layer (FL), reference layer (RL), pinned layer (PL), and pinning antiferromagnetic layer (AFM) for a typical GMR head. The signal transition fields H from the recorded media disk are oriented vertically. These relative orientations also apply to CPP-TMR or CPP-GMR heads.

spacer. In a standard GMR sensor (Fig. 10), the two magnetic layers are the reference layer (RL) and the free layer (FL). Typically, the resistance of the sensor is minimum when RL and FL are parallel ($R = R_{\min}$), while it is maximum when they are anti-parallel ($R = R_{\max} = R_{\min} + \Delta R$), and varies as $R = R_{\min} + (\Delta R/2)(1 - \cos\theta)$, where θ is the angle between the magnetizations.

As mentioned in Section 2.2, the sensor output needs to be linear in order to optimize signal processing and reading density. Therefore the head is engineered so that the easy-axis of the free layer magnetization is oriented along the disk surface with a uniaxial anisotropy H_k. The vector sum of hard bias fields, anisotropy fields, current-induced fields, demagnetization fields and interlayer coupling fields are such that in the zero-field state the FL and RL magnetizations are approximately perpendicular ($\theta = 90°$). See Fig. 11. Angular deviations of the FL magnetization during readback due to the vertical component of the media magnetic field ($\Delta\theta \pm 30°$) result in a quasi-linear output voltage [9].

While the quiescent direction of the FL magnetization is determined by the hard-bias direction (see Section 3.2), the magnetization direction of the reference layer is made to be 'pinned' by direct exchange coupling to an antiferromagnet (AFM). The strength of the exchange energy (typically $J_{ex} > 0.3$ erg/cm^2) at the ferromagnetic/antiferromagnet interface determines the degree of 'pinning' of the RL. This results in an effective pinning field which is inversely proportional to the reference layer magnetization and thickness: $H_{ex} = J_{ex}/M_{RL}t_{RL}$. To further improve the pinning of the RL, every sensor today employs the technique of antiparallel-pinned (AP-pinned) reference layer, where the RL is first exchange coupled to another magnetic layer (the pinned layer PL) via indirect antiferromagnetic exchange mediated by a thin AP-pinning layer (APL) such as Ru [10]. Typically the thickness of Ru is tuned near the first negative (antiferromagnetic) peak of the oscillatory indirect exchange coupling (Ru = 8 Å), resulting in a strong coupling of $J_{ex} \approx 1$ erg/cm^2. Since the RL and the PL are strongly coupled antiparallel to each other, as shown in Fig. 11, they form a rigid magnetic layer whose net magnetization $m_{AP} = M_{RL}t_{RL} - M_{PL}t_{PL}$ can be made arbitrarily small such that the exchange pinning field $H_{ex} = J_{ex}/m_{AP}$ can be greatly increased. Just as important, this AP-pinning technique dramatically reduces the net magnetostatic demagnetization field generated by the RL when the sensor is fabricated to submicron dimensions, which otherwise interferes with proper stabilization of the sensor free layer.

The magnetic response of the free layer is critical to sensor operation. The magnetic thickness of the free layer generally decreases with increased recording density since to achieve a given response (angular deviation $\Delta\theta$), the free layer moment must be matched to the media flux density ($M_r \times t$ where M_r is the remanent media magnetization and t is the media thickness). The media thickness generally scales inversely with recording density, reducing the optimal free layer thickness. With decreasing data bit size, the sensor must also fly closer to the disk to achieve the required resolution. To optimize the overall properties, the free layer is typically a bilayer of CoFe/NiFe$_x$, where the $Co_{90–60}Fe_{10–40}$ provides favorable interface to the Cu spacer layer (see Section 4.2), while the NiFe$_x$ layer ($x < 0.2$) is chosen to reduce and control the intrinsic coercive field H_c, magnetic anisotropy H_k and the magnetostriction λ of the sense layer.

4.2. Optimizing GMR signal

Overall the CIP-GMR signal output voltage of a head is given by $\Delta V = \varepsilon \times (\Delta R/R) \times R_S \times I$, where the efficiency ε is the fraction of the full GMR effect actually utilized by the sensor during the excitation of the free layer as discussed in Section 4.1, and I is the bias current. A typical value for ε is in the range 15–30%, while I is on the order of 3–6 mA. While the basic GMR effect originates in the simple FL/SL/PL trilayer stack, the full GMR head stack comprises numerous additional layers (Fig. 10). Overall, the typical state-of-the-art GMR sensor has a sheet resistance of about $R_S = 25\ \Omega$/square and $\Delta R/R = 15\%$. For a sensor whose stripe height is half of the trackwidth (TW = 2 × SH) this results in a sensor resistance

$R = 50\ \Omega$. For the CIP-GMR geometry, any conducting layer that does not contribute to the GMR response creates an electrical shunting path that reduces the net GMR. In addition, spin-independent scattering sites throughout the structure such as grain boundaries, non-magnetic defects and interfaces also increase the resistance of the sensor without increasing the signal. Hence the optimization of the $\Delta R/R$ for CIP read sensors can be described in three parts: maximizing the positive GMR contributions from spin-dependent scattering, minimizing current shunting (or maximizing current flow through active GMR layers) and eliminating parasitic scattering sites. Each film in the CIP-GMR stack plays a role in determining the total resistance R_S of the sensor, as well as the signal ΔR. In particular, the underlayers (UL) are critical in determining the growth microstructure of the thin films above them, while they must also minimize shunting effects. Their thickness must be generally kept to the practical minimum. Ta underlayers have been used extensively because of their high resistance and high adhesion. However more recently underlayers such as NiFeCr, that significantly increase the grain size of crystalline films, have been found to be highly beneficial to maximize the GMR by reducing parasitic grain boundary scattering [11].

Optimization is necessary as well for the pinning AFM. While the first commercial spin-valves used an insulating NiO AFM [12], the high pinning strength of ordered metallic PtMn has been the preferred AFM material for a number of years [13]. However, the relatively high critical thickness (about 150 Å) below which the pinning is too weak at the operating temperature is an issue both for pinning and for continued scaling to smaller sensor thickness. Consequently alternative antiferromagnets such as IrMn whose critical thickness is much smaller (about 40 Å) [14] or other approaches which do not use an antiferromagnet at all (in this case PL is a hard magnet) [15] are becoming a necessity for implementation into ultra-high density heads.

The Cu spacer layer (SL), because of its high conductivity, can be a major source of shunting unless it is kept as thin as possible. However, as the SL is made thinner, coupling between the FL and the PL (direct exchange coupling through pinholes or magnetostatic Néel coupling due to roughness) must be well controlled for proper sensor operation. Thus the interfaces between the spacer and the magnetic layers, as well as the spacer itself, are carefully engineered to minimize roughness. This can be done, for example, through oxygen plasma exposure of the top of the reference layer and/or low-pressure oxygen exposure during the growth of the SL [16,17]. Through such techniques, the roughness of the critical RL and SL can be controlled, and it is now

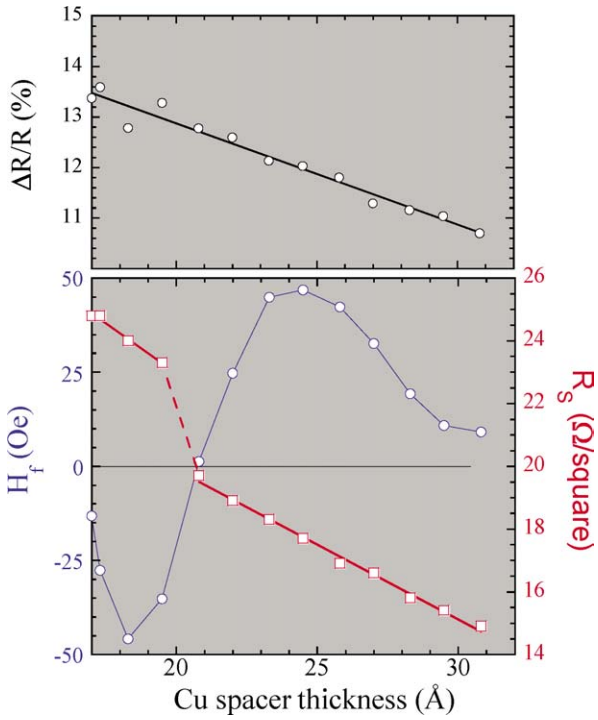

Fig. 12. (a): Magnetoresistance as a function of Cu spacer thickness in a typical GMR sensor multilayer with smooth interfaces. The increase in GMR with thinner Cu is due to the reduction of current shunting through the Cu layer. (b): Coupling field H_f between free and reference magnetic layers (blue curve) as a function of Cu thickness. The coupling field oscillates and becomes negative for Cu below 21 Å due to RKKY coupling. The net multilayer sheet resistance R_S (red curve) also increases with thinner Cu, which will increase the sensor output voltage. The discontinuous increase of R_S for Cu below 21 Å is due to the antiparallel orientation of the free and reference layer magnetizations in this region (negative coupling field), while the orientation is parallel for thicker Cu (positive coupling field). The final relative orientation in a properly biased sensor is always orthogonal, as shown in Fig. 11.

common to decrease the thickness of the SL to about 20 Å and make use of the antiferromagnetic RKKY coupling across Cu to reduce the net coupling (RKKY + magnetostatic) to a very small or negative value; see Fig. 12, which shows the relationship between interlayer coupling field, sensor sheet resistance, and magnetoresistance as a function of Cu spacer thickness [18]. Similarly, any shunting through the cap layers (CL) must also be eliminated. Thus, while the cap layer, in contact with the FL, must be carefully optimized to maximize GMR and optimize the FL magnetostriction, a high-resistance material such as Ta or Al_2O_3 is preferable as the main constituent of high-resistance cap layers [19].

4.3. Contiguous junction stabilization

CIP sensor performance requires that the lead layer and the stabilization layer be in contact and in perfect alignment with the edges of the sense region. This alignment is achieved with a fabrication process that creates a contiguous junction between the sensor edges and the stabilization and lead edges. Misalignment of the lead region to the sense region creates contact resistance. Misalignment of the stabilization layer edge to the sense region reduces coupling of the hard bias stabilization field into the free layer. The self-aligned contiguous junction process is described in Fig. 13. The process uses a single optical lithography step to define the sensor width and a set of additive and subtractive processing steps [20]. After the film layers of the sense region are deposited, a bi-layer resist stencil is lithographically formed followed by ion milling to define the edges of the sensor width by subtractive removal of the open regions of the sense materials. Next, an additive deposition of a hard ferromagnetic layer and then a lead material are deposited onto both the resist and the regions where the sense layers were removed. The resist is dissolved resulting in the liftoff of the lead and hard ferromagnetic material above the sensor and the formation of a junction at the edge of the sense layers with the hard ferromagnetic stabilization layer and the lead layer. After the junction is formed a second lithography step with subtractive ion milling is used to define the depth or height of the sensor. A processed sensor with 200 nm width and abrupt contiguous junctions is shown in Fig. 14.

4.4. Reliability

Notwithstanding the small scale and complexity of the thin film GMR read sensor, it has proven to be remarkably robust and reliable in products. There are several areas that make the GMR sensor vulnerable to attack and degradation. First, with a typical thermal time constant of well under 1 nanosecond the sensor is very sensitive to electrostatic discharge (ESD) and current stresses. This means that accidental current bursts lasting only a few nanoseconds can cause the sensor films to reach very high temperatures, degrading their magnetic and electrical properties and in some cases causing sensor melting. This sensitivity has driven head manufacturing to adopt tooling and processes that produce very low levels of ESD. It has also forced careful engineering of potential electrostatic events in hard disc drives. This sensitivity has also driven electronic component designs which limit current transients and cross talk during disk-drive operations. Second, the thin films which compose the sensor multilayer must maintain their nanoscale microstructures over the device lifetime. This requires that diffusion at the film interfaces and at grain boundaries be minimal at typical device operating temperatures of 100 °C. Third, the thin films in the sensor are vulnerable to chemical attack and atmospheric corrosion if exposed to ambient humidity. The completed sensors, at the air-bearing

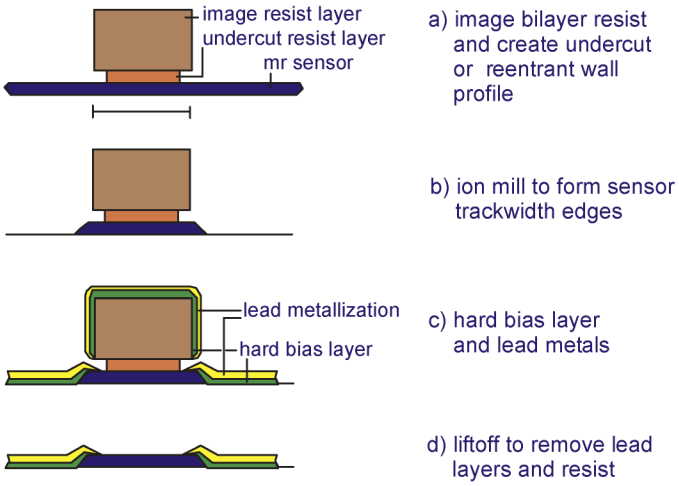

Fig. 13. Self-aligned contiguous junction process used to form a GMR sensor with longitudinal hard bias.

surface, have a carbon overcoat of 3–4 nm thickness which provides some degree of environmental protection. Considerable effort in understanding and controlling the head-disk interface is critical to the long-term reliability of the recording system.

4.5. CIP sensor limitations

As sensor dimensions continue to decrease, several factors are contributing to performance limitations for CIP-GMR sensors, which necessitate further evolution in sensor design. First, as density increases both RW and TG must decrease. Since the sensor current travels parallel to RW, this implies that the length of the sensors must continuously decrease, and therefore the sensor height above the disk (SH) must also decrease to keep the sensor resistance R and the signal ΔR constant. If this simple scaling cannot be accomplished, or if edge effects reduce the effective signal, then the intrinsic GMR ratio must increase proportionally to keep the output signal constant. Also, as the volume of the sensor decreases, the influences of sensor edges increases, exposing limitations related to damage of the sensor during fabrication. In particular, RW-defining edges are susceptible to ion-milling damage, while SH-defining edges are susceptible to both ion milling and lapping damage (due to the formation of the air-bearing surface), which again must be offset by an increase in the GMR coefficient. However, the GMR of practical spin-valve devices appears to be limited to 20% at the most, close to current technology. Furthermore, as TG decreases, it becomes more difficult to fit low-resistance electrical leads between the shields, which increases the parasitic resistance and reduces the effective signal. Finally, hard-bias stabilization of the sensor (without decreasing the sensitivity) is becoming more challenging due to the large demagnetization fields in small sensors. Consequently, it is unlikely that traditional scaling projection (as shown in Fig. 7) can be realized without substantial changes in head geometry, design and materials. Thus, new technological "paradigm shifts" are still required to continue the evolution of the read heads towards 1 $\mathrm{Tb/in^2}$ recording.

5. Current-perpendicular (CPP) heads

To overcome the limitations of the CIP geometry described above, a sensor geometry in which the current flows perpendicular to the plane of the shields (Fig. 15) has several significant advantages: (1) the magnetic shields can naturally be used as electrical leads for the sensor, which eliminates the need to electrically insulate the sensor from the shield with a gap insulator, and also eliminates the need for separate lead structures; (2) the sensor current travels perpendicularly to the sensor multilayer, which eliminates signal-shunting paths in non-active layers (instead the layers will contribute to in-series parasitic resistance); (3) the sensor dimensions (RW and SH) now constitute the cross-sectional area A of the sensor. Thus R_{Sensor} increases as the sensor dimensions are reduced. Therefore in this geometry the relevant resistance metric is the perpendicular resistance $\times$ area (RA) product of the sensor stack material, and $R_{\mathrm{Sensor}} = \mathrm{RA}_{\mathrm{Stack}}/A_{\mathrm{Sensor}}$. As recording bit density increases, A_{Sensor} will decrease and consequently $\mathrm{RA}_{\mathrm{Stack}}$ must also decrease if the sensor impedance is to remain approximately constant. Thus among CPP sensors we must first consider sensors with high RA (tunnel junctions, where the spacer layer in Fig. 15 is a thin insulator) and then, for still higher densities, sensors with lower RA (GMR spin-valves, where the spacer layer is metallic). Note that from a magnetic properties point of view, CPP sensor stack design considerations are nearly identical to those described above for CIP-GMR sensors.

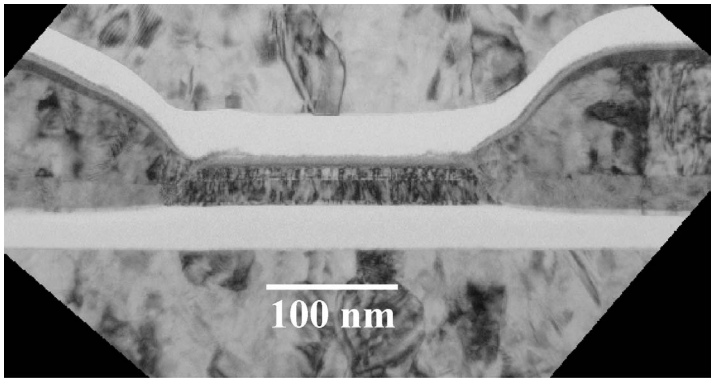

Fig. 14. Example of completed GMR sensor with sensor read width RW = 200 nm. The various regions can be identified by comparing to the schematic in Fig. 9.

5.1. Tunnel-magnetoresistive sensors and heads

Magnetic tunnel junctions (MTJ), although investigated well before GMR spin-valves, have attracted considerable interest only since 1994 when large magnetoresistance at room temperature was first observed [21]. This illustrates the fact that, as a rule, the performance of MTJs, and tunnel barriers in particular, are much more sensitive to fabrication conditions than GMR spin-valves, and thus deposition techniques are more difficult to optimize. Since then MTJs have mainly been associated with higher impedance device applications such as magnetic random-access memory (MRAM) and other spintronics devices. These applications, along with the physics of MTJs are discussed in more detail elsewhere in this issue. Yet, MTJs also make attractive sensors for high-density heads because of the large signal which results from large tunnel-magetoresistance ratios (TMR) which have been observed over the last few years (>50% for CoFe/Al_2O_3/CoFe and now > 200% for CoFe/MgO/CoFe junctions). On the other hand, the large MTJ sensor resistance and output is accompanied by large noise, including shot noise which is specific to tunneling sensors [22]. In addition, the high RC time constant of a high-impedance TMR sensor results in an unacceptable decrease in attainable sensor bandwidth (typically 200 MHz – 1 GHz). Therefore, the SNR for high-density MTJ head sensors is sufficiently high for head applications only when the RA ratio is sufficiently small (<10 Ω-μm^2) [23]. Thus only low-resistance MTJs are suitable for recording heads. In fact, MTJs have very recently begun to appear in product-level recording sensors, and therefore CPP-TMR sensors are on the verge of becoming a significant alternative to CIP-GMR sensors [24].

In TMR devices with conventional insulating barriers (such as amorphous Al_2O_3), a low-resistance device can be obtained either by decreasing the thickness of the tunnel barrier, or by decreasing the tunnel barrier height. This is well described by the Brinkmann model of the tunneling conduction process [25]. Considerable effort has been expanded to perfect the thin-film techniques to create the thinnest possible barriers free of pinhole shorts that degrade the magnetoresistance, as well as tailor the composition and interfaces of the tunnel barriers to reduce the effective barrier height [26]. The best results obtained to date have resulted in a few Ω-μm^2 RA product with about 20% MR ratios. Of course, as shown in Fig. 16, if the barrier is fabricated ever thinner, lower RA products can be obtained at the expense of lower MR ratio, as the overlap of electron wave functions, barrier

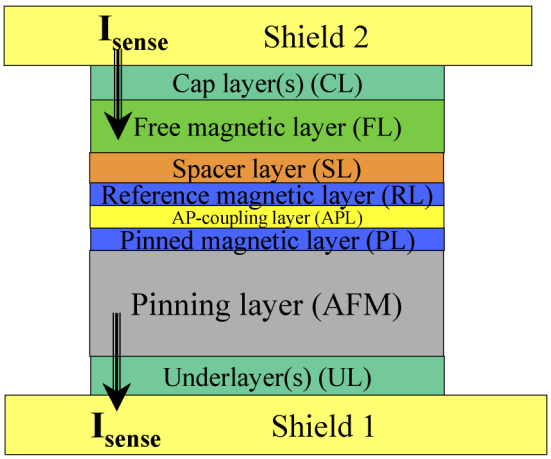

Fig. 15. Disk-view schematic of typical thin-film multilayer stack for a CPP sensor. The current flows vertically between the shield regions.

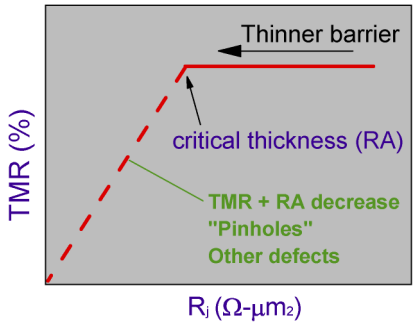

Fig. 16. Typical TMR behavior vs. junction specific resistance $R_j = R \times A$ for low-resistance TMR sensor. Below a critical barrier thickness (critical RA), the TMR decreases linearly due to spin-independent shunting of the current through barrier defects.

degradation, and metallic pinholes combine to shunt the TMR effect. More recently, it has been predicted theoretically [27] and later verified experimentally [28] that band-matching effects between certain combinations of crystalline insulators and crystalline magnetic metals can result in huge MR ratios and effective barrier heights much smaller than the bulk value of the barrier material. Surprisingly, among the films grown by sputtering, the best barrier and interface properties published to date have been obtained by crystallizing a thin MgO film on amorphous CoFeB alloy films, followed by high-temperature annealing which crystallizes a CoFe-rich film in contact with the crystalline MgO. TMR values of >150% have been obtained at about 2 Ω-μm^2 in that case [29].

These results are highly encouraging for the future of TMR sensors in recording heads, given the fact that tunnel-based devices have some potential advantages over metallic-only devices. In particular, because the TMR effect originates in an atomic scale region on either side of the tunnel barrier, and because the tunnel barrier is by far the greatest resistivity layer of the stack, the RA product and TMR of the sensors are (in principle) largely independent of the details in the rest of the stack. That is, the optimization of the entire stack (for example adjusting layer thicknesses to optimize magnetic properties, or the choice of antiferromagnets) should have no significant effect on the TMR. In reality, of course, the quality and properties of tunnel barriers in the ultrathin regime (<10 Å) is highly sensitive to interface roughness, crystalline texture and interface mixing. Therefore the growth of the entire sensor stack up to and next to the barrier is most critical in determining the final sensor properties. For example, while the S1 shield surface is covered by a thick amorphous insulator (generally Al_2O_3) prior to CIP-GMR sensor deposition, the deposition of the CPP-TMR stack occurs directly atop the metal shield surface. Thus shield surface preparation (CMP planerization, ion cleaning, etc.) is an important step, essential for successful sensor integration. Also, when fabricating CPP-TMR sensors, care must also be taken to avoid any shorting at the sensor edges due to metallic re-deposition of ion-milled products. For example, even at a low RA product of 2 Ω-μm^2, a sensor of 50 × 50 nm size will have a resistance of 800 Ω, with a perimeter of 200 nm, and therefore even modest metallic redeposition can reduce the net resistance (and the signal) significantly. Nevertheless, the high TMR, favorable CPP geometry, and design flexibility inherent in MTJ-based heads constitute an attractive package for the next generation head sensor technology.

5.2. CPP-GMR sensors and heads

Metallic GMR spin-valves are also of interest in a CPP geometry. While the intrinsic $\Delta R/R$ of a CPP-GMR spin-valve is comparable to the CIP case, here the RA product of the active sensor is much lower (ΔRA = 1 mΩ-μm^2 and RA < 10 mΩ-μm^2 for a typical PL/spacer/FL spin-valve) [30]. Consequently the parasitic resistance of all the other layers in the stack (typically $R_{\text{paras}}A$ = 30–50 mΩ-μm^2, in large part due to the antiferromagnet) is actually several times larger and therefore the net $\Delta R_S/(R_S + R_{\text{paras}})$ is typically small (<2%). Because of the low resistance, a large sensor current density will be needed to create a given output voltage level compared to CPP-TMR. For example, for RA = 50 mΩ-μm^2, a 50 nm × 50 nm sensor has a resistance of 20 Ω, and for a GMR value of 2%, each 1 mV of output signal ΔV requires a bias current of 2.5 mA, which corresponds to a current density of 10^8 A/cm^2. Compared to CPP-TMR, noise contributions are smaller for CPP-GMR because of the absence of shot noise, and similar to CIP-GMR (Johnson noise only). However, due to the CPP geometry the thermal sinking of the sensor to the shields will improve thermal characteristics at small dimensions compared to CIP-GMR. Generally, the low resistance of CPP-GMR sensor compared to CPP-TMR will decrease the resistance and therefore will improve the attainable bandwidth at the smallest sensor dimensions, as long as sufficient GMR signal is maintained [31]. Consequently, the optimization of GMR is an important challenge for future CPP sensors. It has already been demonstrated that appropriate laminations in the magnetic layers can significantly increase ΔRA [32]. However, further improvements are still required to increase the effective signal in CPP-GMR sensors. For example, the use of high-resistance, high spin-polarization magnetic alloys such as ferromagnetic Heusler alloys has already resulted in encouraging performance improvements [33]. Another remarkable way to increase both RA and $\Delta R/R$ in CPP-GMR sensor is through the use of current-confinement techniques such as the use of as nano-oxide layer (NOL) within the spin-valve stack [34]. In that case, the resistance of the high-GMR spin-valve is increased selectively in contrast to the parasitic layer resistances, increasing the effective $\Delta R/R$ of the structure. Note that in that case the effect is purely geometrical, and thus the notion of ΔRA is no longer applicable since the current is not uniform and therefore the effective sensor area is not well defined.

5.3. Insulated contiguous junction stabilization

As indicated earlier, the CPP geometry allows the omission of separate electrical leads as the shields themselves constitute the electrical connections to the sensor. However stabilization of the sensor is still required, and a conventional hard-bias approach thus requires that the hard-magnet material be insulated from the sensor. In the CPP structure the leads are now the top and bottom shield and the hard magnet bias material must be insulated from the edges of sense layer forming an insulating contiguous junction, as shown in Fig. 17(a), (b). Fabrication of the CPP structures is identical to the process for forming a CIP structure with the only change being in the additive deposition step (Fig. 13(c)). The insulating contiguous junction structure is

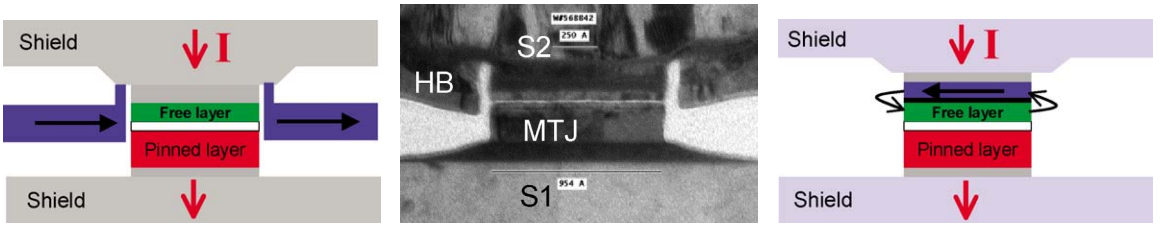

(a) (b) (c)

Fig. 17. (a) Schematic of CPP-TMR sensor with insulating contiguous-junction stabilization; (b) TEM micrograph of corresponding TMR head structure with sensor read width RW = 100 nm; (c) schematic of in-stack bias stabilization scheme for CPP sensor. The hard bias material (blue) is deposited above the free layer within the sensor multilayer stack and forms a closed flux magnetic structure with the free layer.

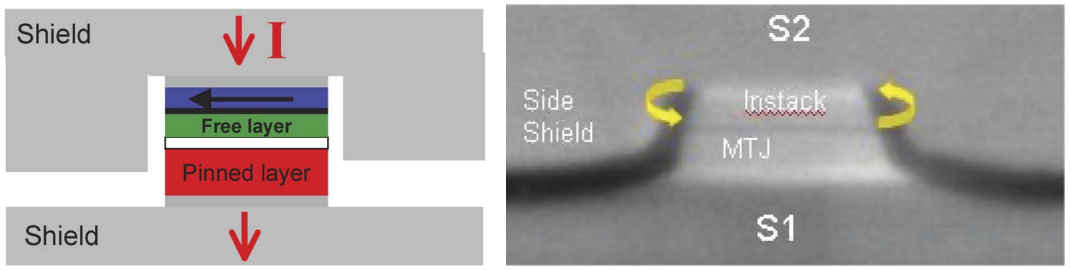

(a) (b)

Fig. 18. (a) Schematic of CPP sensor with in-stack bias and side-shield that drape down conformally on the sides of the sensor. (b) SEM micrograph of corresponding CPP-TMR head structure.

formed by changing the CIP deposition step from 'hard ferromagnet + leads' to 'insulator + hard ferromagnet + insulator'. The first insulator thickness is typically 4–8 nm and the second insulator thickness is typically 8–15 nm. The hard magnet can also be electrically connected to the top shield by substituting the second insulator deposition by a non-magnetic metal such as Ta or Rh.

5.4. In-stack biasing and conformal shielding in CPP geometry

A possible alternative to the ICJ for CPP sensors is to place the hard magnet directly in the sensor stack, in close proximity to the free layer, as shown in Fig. 17(c). The insulator thickness between the shields is now comparable to the stack height of all the layers in the sense region or ~ 40 nm. Upon definition of the sensor RW, edge magnetostatic coupling between the hard magnet and the free layer effectively biases the sensor if the geometry and materials performance are optimized: The bias magnet must be sufficiently close to the free layer but without direct ferromagnetic or Néel coupling to it, and the hard magnet itself must be well stabilized (for example by pinning to an antiferromagnet) [35].

One advantage of the in-stack bias approach is that the fabrication of the sensor structure is greatly simplified (no contiguous junction process—RW definition and stabilization are one and the same process). Another advantage is that, in the absence of electrical leads and hard bias on the sides of the sensor, the magnetic shield which is normally electroplated on top of the stack can be made to be conformal with the sensor itself, thus providing side shielding to the sensor (Fig. 18(a), (b)) which can improve narrow-track, high-track-density performance [36]. In the case of AF-pinned in-stack bias layer, the challenge is to balance the thickness of the in-stack bias layer (thicker bias layer provides more magnetic flux for free layer stabilization) and the strength of the pinning (thicker bias layer results in a decrease of the pinning exchange field). Fig. 19 shows the improvement obtained for experimental microtrack profiles (data readback width in the cross-track direction) by using a conformal shielding approach, which then allows for a higher density of recorded tracks for a given sensor trackwidth.

5.5. Spin-torque effects and other limitations

For all-metallic CPP sensors with low RA, as discussed is Section 5.2, the sensor output voltage must be maintained either by increasing the sense current or by increasing the sensor GMR. Increasing the current has several consequences, including increasing the sensor temperature (although in the CPP geometry the shields act as efficient heat sinks), causing electromigration at multilayer interfaces, and increasing the self-ampere field which tends to drive the sensor in a vortex domain state [37]. The

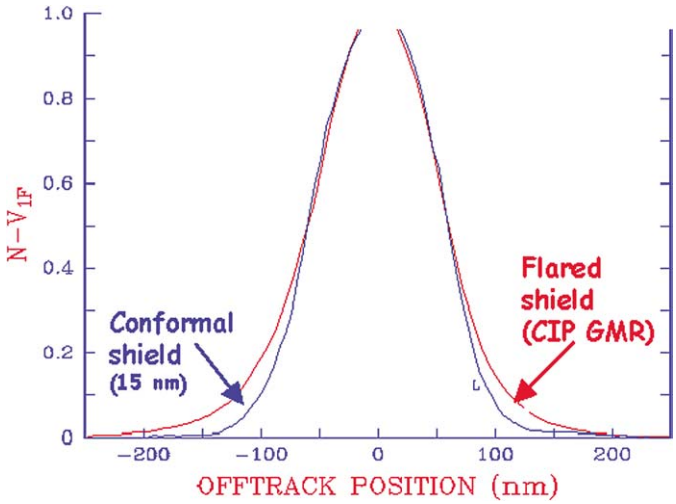

Fig. 19. Microtrack profile of read response from 100 nm-wide CIP-GMR with standard contiguous-junction hard bias and flared shield (red curve) and CPP-TMR with in-stack bias and conformal shield (blue curve). The decreased skirt width in the CPP case with conformal shield corresponds to an effective decrease in the sensor read width (RW).

most serious limitation on sense current, however, is the effect of spin transfer which causes the sense layer to become unstable under the influence of a current spin-polarized by the reference layer. In a simple CPP-GMR spin-valve, this instability, along with the rapid increase in sensor noise has been observed for current densities as low as 1×10^7 A/cm^2 [38]. A solution for this is the use of dual spin-valves, where the existence of two reference layers symmetric about the pinned layer result in a drastic increase in the usable sense current [39]. The disadvantage of dual spin-valves is the increased total sensor stack thickness which is a challenge to the continued scaling of sensor dimensions. In fact, it is ultimately this continued scaling which poses the greatest challenge to ferromagnetic GMR or TMR sensor: As the total volume of the free layer decreases, thermally activated noise of the magnetization direction (also known as mag-noise), even in a stabilized sensor, becomes an increasing problem [40]. Currently, it is difficult to conceive of practical ferromagnetic sensors with trackwidths much below 30 nm.

6. Future head technologies

6.1. Future storage technologies and heads

Several new storage technologies are currently being explored to allow the continued increase of achievable storage densities and to circumvent the challenge of media superparamagnetism (spontaneous thermally activated magnetic reversal of recorded bits) which will eventually afflict scaled-down conventional media: (1) Perpendicular magnetic recording increases bit stability with a larger volume and perpendicular orientation [41]; (2) Thermally assisted recording allows higher stability media to be recorded by the addition of thermal energy during the recording process [42]; and (3) Patterned bit media increases bit stability by isolating each bit within its own magnetic island [43]. In all these cases, however, the magnetic read sensor performs the same function, namely detects magnetic transition by measuring the vertical component of the magnetic field above the disk. Consequently, the basic geometry and functionality of the read sensor will not necessarily be modified by the transition to any of these technologies. Instead, magnetic characteristics of the sensor free layer will need to be matched to the characteristics of the specific media, such as the total magnetic flux variation resulting from each bit transition. In fact, perpendicular media actually impacts the read sensor in a favorable manner. Specifically, the presence of a soft underlayer at the base of the perpendicular media layers better confines the flux, in comparison with longitudinal media, coming from the transitions. As a result the magnetic detection width of the sensor more closely approximates the actual physical width of the sensor. For a perpendicular recording system, a larger lithography for forming the physical sensor width for a given magnetic track width is possible making sensor fabrication more manufacturable [44]. The central question in each case is whether new geometrical constraints at each recording density target, such as trackwidth, shield-to-shield spacing, and media magnetic field will be compatible with standard ferromagnetic materials and GMR or TMR-type sensors and their associated issues at small dimensions (see Section 5.5), or whether new sensor types will altogether be required.

6.2. Future sensor technologies

New technologies with relevance to recording head sensors are actively being pursued. As it has been described above, as bit dimensions continue to shrink, the requirements for sensors are smaller intrinsic impedance per unit area, higher signal levels, and immunity from scaling issues such as spin-torque noise and thermal mag-noise. The emerging field of spin-electronics, combining magnetic materials with spin control and semiconductor functionality, is fertile ground for the exploration of new recording head paradigms. For example, devices such as the spin-valve transistor and magnetic tunnel transistor, which rely on the spin-filtering of hot-electrons in three-terminal devices have received some attention due to large magneto-conductance effects ($>100\%$) observed [45,46]. Nevertheless, theses devices offer total resistances which are similar to CPP-TMR sensors, and the recent observations of $>200\%$ MR in TMR sensors reduce the perceived advantages that may be gained from these new technologies. In addition, all magnetic-based sensors will need to be integrated with a write head, with magnetic shields to improve resolution, and will also suffer from the same scaling limitations in terms of thermal instabilities and mag-noise. To avoid these latter issues, a very different approach is to design the magnetic sensor without any ferromagnetic material, therefore eliminating the issues of magnetic thermal noise and sensor stabilization. For example, the extraordinary magneto-resistance (EMR) sensor, based on the Lorentz deviation of electrons in shunted high-mobility semiconductor heterostructures, offers many of the required sensor characteristics [47]. However, significant challenges remain to achieve scaling to sizes below 50 nm and adapted to a slider geometry on a recording head. Nevertheless, it represents an intriguing example of new physics and new magnetic sensing principles which can potentially keep the magnetic recording head sensor marching down its path toward the nanometer-scale.

7. Conclusions

Magnetic recording head sensors based on current-in-plane magnetoresistive multilayers have continuously evolved and improved to meet the requirements of ever-increasing areal density recording. Yet, the severe geometrical constraints which accompany the highest recording densities have stretched today's processing capabilities and exposed physical limitations on the magnetic and magnetotransport properties. New current perpendicular to plane (CPP) geometries show processing and performance advantages which will allow, for now, the continued progress of head sensors with tunnel-magnetoresistance and CPP-GMR sensors. Because the processing of critical dimensions has now caught up with that of the semiconductor industry, further lithographic progress will now simply follow the current state of the art. The most daunting challenge for future read sensor technology will be thermally-activated magnetic noise at small dimensions, which will limit the smallest practical ferromagnetic sensor volume, or necessitate a transition to non-magnetic sensor technologies.

Acknowledgements

Many thanks to the following colleagues for their contributions and critical comments: Alex Zeltser, Lamar Nix, Michael Ho, Ching Tsang, Neil Smith, Wen Lee, Matt Carey, Stefan Maat, Jordan Katine, Ian McFadyen, and Bruce Gurney.

References

[1] B.A. Gurney, M. Carey, C. Tsang, M. Williams, S.S.P. Parkin, R.E. Fontana Jr., E. Grochowski, M. Pinarbasi, T. Lin, D. Mauri, in: B. Heinrich, J.A.C. Bland (Eds.), Ultrathin Magnetic Structures IV: Applications of Nanomagnetism, Springer-Verlag, Berlin/New York, 2005, pp. 149–174.
[2] C.H. Tsang, R.E. Fontana, T. Lin, D.E. Heim, B.A. Gurney, M.L. Williams, IBM, J. Res. Development 42 (1998) 103–116.
[3] T.D. Howell, P.A. McEwen, A. Patapoutian, J. Appl. Phys. 87 (2000) 5371–5376.
[4] R.E. Fontana, J. Katine, M. Rooks, R. Viswanathan, J. Lille, S. MacDonald, E. Kratschner, S. Nguyen, N. Robertson, P. Kasiraj, IEEE Trans. Magn. 38 (1) (2002) 95.
[5] C.H. Bajorek, S. Krongelb, L.T. Romankiw, D.A. Thompson, in: 20th Annual AIP Conf. Proc., American Institute of Physics, 1974, p. 24.
[6] M.T. Krounbi, W.J. Van Gestel, P.-K.Wang, U.S. patents #5,005,096 and #5,018,037 (1991).
[7] J.C. Mallinson, Horizontal Biasing Techniques, Academic Press, San Diego, 1996 (Chapter 6).
[8] A. Tsoukatos, S. Gupta, D. Marx, J. Appl. Phys. 79 (1996) 5018.
[9] D.E. Heim, R.E. Fontana, C.H. Tsang, V. Speriosu, B.A. Gurney, M.L. Williams, IEEE Trans. Magn. 30 (1994) 316–321.
[10] R.E. Fontana, B. Gurney, T. Lin, V. Speriosu, C. Tsang, D. Wilhoit, U.S. patent #5,701,223.
[11] W.Y. Lee, T. Lin, D. Mauri, R.W. Wilson, U.S. patent # 6,141,191 (2000).
[12] M. Pinarbasi, S. Metin, H. Gill, M. Parker, B. Gurney, M. Carey, C. Tsang, J. Appl. Phys. 87 (2000) 5714.

[13] M. Saito, N. Hasegawa, F. Koike, H. Seki, T. Kunyama, et al., J. Appl. Phys. 85 (1999) 4928.
[14] H. Yoda, H. Iwasaki, T. Kobayashi, A. Tsutai, M. Sahashi, IEEE Trans. Magn. 32 (1996) 3363.
[15] K.R. Coffey, B. Gurney, D. Heim, H. Lefakis, D. Mauri, V. Speriosu, D. Wilhoit, U.S. patent #5,583,725 (1996).
[16] S. Sant, M. Mao, J. Kools, K. Koi, H. Iwasaki, M. Sahashi, J. Appl. Phys. 89 (2001) 6931–6933.
[17] W. Kula, A. Zeltser, U.S. patent #6,700,754 (2004).
[18] A. Zeltser, Private communication (2005).
[19] T. Lin, D. Mauri, Appl. Phys. Lett. 78 (2001) 2181–2183.
[20] R.E. Fontana, S. MacDonald, C. Tsang, T. Lin, et al., IEEE Trans. Magn. 32 (5) (1996) 3440.
[21] J.S. Moodera, L.R. Kinder, T.M. Wong, R. Meservey, Phys. Rev. Lett. 74 (1995) 3273.
[22] K.B. Klaasen, X.Z. Xing, J.C.L. van Peppen, IEEE Trans. Magn. 40 (2004) 195–202.
[23] M.L. Mallary, in: 1999 Digest of IEEE Intermag Conference, May 18–21, 1999, p. BP11;
K. Ohashi, K. Hayashi, K. Nagahara, K. Ishihara, E. Fukami, J. Fujikata, S. Mori, M. Nakada, T. Mitsuzuka, K. Matsuda, H. Mori, A. Kamijo, H. Tsuge, IEEE Trans. Magn. 36 (2000) 2549.
[24] S. Mao, F. Liu, B. Xu, H. Xi, P. Lu, J. Shen, X. Chen, C. Chang, B. Miller, M. Patwari, B. Pant, J. Loven, J. Gadbois, B. Cross, J. Ding, P. Ryan, in: 2005 TMRC Conference, Palo Alto, paper A2; IEEE Trans. Magn., submitted for publication.
[25] W.F. Brinkmann, R.C. Dynes, J.M. Rowell, J. Appl. Phys. 41 (1970) 1915.
[26] J.R. Childress, M.M. Schwickert, R.E. Fontana, M.K. Ho, P.M. Rice, B.A. Gurney, J. Appl. Phys. 89 (2001) 7353;
J. Fujikata, T. Ishi, S. Mori, K. Matsuda, K. Mori, H. Yokota, K. Hayashi, M. Nakada, A. Kamijo, K. Ohashi, J. Appl. Phys. 89 (2001) 7558;
W. Jianguo, P. Freitas, E. Snoeck, X. Batlle, J. Cuadra, IEEE Trans. Magn. 38 (2002) 2703.
[27] W.H. Butler, X.-G. Zhang, T. Schulthess, Phys. Rev. B 63 (2001) 054416.
[28] S. Yuasa, A. Fukushima, T. Nagahama, K. Ando, Y. Suzuki, Jap. J. Appl. Phys. 43 (2004) L588;
S.S.P. Parkin, C. Kaiser, A. Panchula, P. Rice, B. Hughes, M. Samant, S. Yang, Nature Mater. 3 (2004) 862.
[29] K. Tsunekawa, D. Djayaprawira, M. Nagai, H. Maehara, S. Yamagata, N. Watanabe, Appl. Phys. Lett. 87 (1) (2005), art. no. 072503.
[30] W. Pratt, S. Steenwyk, S. Hsu, W. Chiang, A. Schaefer, R. Loloee, J. Bass, IEEE Trans. Magn. 33 (1997) 3505–3510.
[31] M. Takagishi, K. Koi, M. Yoshikawa, T. Funayama, H. Iwasaki, M. Sahashi, M. Takagishi, IEEE Trans. Magn. 38 (2002) 2277.
[32] H. Yuasa, M. Yoshikawa, Y. Kamiguchi, K. Koi, H. Iwasaki, M. Takagishi, M. Sahashi, J. Appl. Phys. 92 (2002) 2646.
[33] M. Saito, N. Hasegawa, Y. Ide, T. Yamashita, Y. Hayakawa, Y. Nishiyama, M. Ishizone, S. Yanagi, K. Honda, N. Ishibashi, D. Aoki, H. Kawanami, K. Nishimura, J. Takahashi, A. Takahashi, in: Digests of Intermag 2005 Conference, Nagoya, IEEE, 2005, paper FB-02.
[34] H. Oshima, K. Nagasaka, Y. Seyama, A. Jogo, Y. Shimizu, A. Tanaka, Y. Miura, IEEE Trans. Magn. 39 (2003) 2377.
[35] J.R. Childress, M. Ho, R. Fontana, M. Carey, P. Rice, B. Gurney, C. Tsang, IEEE Trans. Magn. 38 (2002) 2286.
[36] M.K. Ho, C. Tsang, J. Childress, R. Fontana, J. Jatine, K. Carey, IEEE Trans. Magn. 40 (2004) 189.
[37] K. Ishihara, M. Nakada, E. Fukami, K. Nagahara, H. Honjo, K. Ohashi, IEEE Trans. Magn. 37 (2001) 1687.
[38] J.G. Zhu, N. Kim, Y. Zhou, Y. Zheng, J. Chang, K. Ju, X. Zhu, R.M. White, IEEE Trans. Magn. 40 (2004) 2323;
N. Smith, J.A. Katine, J.R. Childress, M.J. Carey, in: Intermag Conference 2005, Nagoya, paper FB-04; IEEE Trans. Magn. (2005), in press.
[39] J.R. Childress, M.J. Carey, S.I. Kiselev, J.A. Katine, S. Maat, N. Smith, in: 2005 MMM Conference, San Jose, paper HB-05; J. Appl. Phys. (2006), in press.
[40] N. Smith, P. Arnett, IEEE Trans. Magn. 38 (2002) 32.
[41] H.N. Bertram, M. Williams, IEEE Trans. Magn. 36 (2000) 4–9.
[42] J.J.M. Ruigrok, R. Coehoorn, S. Cumpson, H. Kesteren, J. Appl. Phys. 87 (2000) 5398.
[43] D. Weller, A. Moser, IEEE Trans. Magn. 35 (1999) 4423.
[44] C. Tsang, S. MacDonald, G. Samadi, J. Katine, M. Cyrille, A. Driskill-Smith, M. Ho, J. Moore, W. Weresin, P. Arnett, E. Marinero, D. Druist, M. Pinarbasi, A. Polcyn, K. Takano, Y. Ikeda, H. Do, M. Best, A. Moser, IEEE Trans. Magn. 40 (2004) 295–300.
[45] D.J. Monsma, J.C. Lodder, T.J.A. Popma, B. Dieny, Phys. Rev. Lett. 74 (1995) 5260–5263.
[46] S. van Dijken, X. Jiang, S.S.P. Parkin, Appl. Phys. Lett. 80 (2002) 3364–3366.
[47] S.A. Solin, D.R. Hines, A.C.H. Rowe, J.S. Tsai, Yu.A. Pashkin, S.J. Chung, N. Goel, M.B. Santos, Appl. Phys. Lett. 80 (2002) 4012.